PLOS ONE

RESEARCH ARTICLE

Endosomal structure and APP biology are not altered in a preclinical mouse cellular model of Down syndrome

Claudia Cannavo[1,2], Karen Cleverley[2], Cheryl Maduro[2], Paige Mumford[1], Dale Moulding[3], Elizabeth M. C. Fisher[2¶], Frances K. Wiseman[1¶*]

1 UK Dementia Research Institute, UCL Queen Square Institute of Neurology, London, United Kingdom, **2** Department of Neuromuscular Diseases, UCL Queen Square Institute of Neurology, London, United Kingdom, **3** Light Microscopy Core Facility, UCL Great Ormond Street Institute of Child Health, London, United Kingdom

¶ Membership of the LonDownS Consortium is provided in the Acknowledgments.
* f.wiseman@ucl.ac.uk

Citation: Cannavo C, Cleverley K, Maduro C, Mumford P, Moulding D, Fisher EMC, et al. (2022) Endosomal structure and APP biology are not altered in a preclinical mouse cellular model of Down syndrome. PLoS ONE 17(5): e0262558. https://doi.org/10.1371/journal.pone.0262558

Editor: Stephen D. Ginsberg, Nathan S Kline Institute, UNITED STATES

Received: December 21, 2021

Accepted: April 21, 2022

Published: May 11, 2022

Data Availability Statement: All relevant data are within the paper and Figshare: DOI 10.6084/m9.figshare.17316434.

Funding: C.C. was funded by an Alzheimer's Society PhD studentship (AS-PhD-16-003 2017-20) awarded to F.K.W and E.M.C.F. https://www.alzheimers.org.uk/ F.K.W holds an Alzheimer's Research UK Senior Research Fellowship (ARUK-SRF2018A-001). https://www.alzheimersresearchuk.org/ F.K.W. is also supported by the UK Dementia Research Institute

Abstract

Individuals who have Down syndrome (trisomy 21) are at greatly increased risk of developing Alzheimer's disease, characterised by the accumulation in the brain of amyloid-β plaques. Amyloid-β is a product of the processing of the amyloid precursor protein, encoded by the *APP* gene on chromosome 21. In Down syndrome the first site of amyloid-β accumulation is within endosomes, and changes to endosome biology occur early in Alzheimer's disease. Here, we determine if primary mouse embryonic fibroblasts isolated from a mouse model of Down syndrome can be used to study endosome and APP cell biology. We report that in this cellular model, endosome number, size and APP processing are not altered, likely because *APP* is not dosage sensitive in the model, despite three copies of *App*.

Introduction

Individuals with Down syndrome (DS), which is caused by trisomy of human chromosome 21 (Hsa21), have a high risk of developing early onset Alzheimer's disease (AD). One of the earliest neuropathological features of AD in people who have DS is the intracellular accumulation of amyloid-β in the brain, followed by the accumulation of extracellular amyloid-β plaques [1]. Amyloid-β is a product of the *APP* gene that is encoded on Hsa21. Clinical-genetic studies indicate that three copies of *APP* are both sufficient and necessary for the development of early onset AD in people who have DS and in the general population. However, growing evidence suggests that other genes on Hsa21 can affect APP/amyloid-β, for example via modulation of endosomal biology [2].

APP follows the central secretory pathway. Full-length APP is synthesised in the endoplasmic reticulum, transported to the Golgi and then to the plasma membrane [3, 4]. From there, APP is internalized through endocytosis and either recycled to the plasma membrane or Golgi, or directed for degradation to the endo-lysosomes [5–7]. Where APP lies in the cell is important for its degradation. APP mainly undergoes two alternative types of processing,

(UKRI-1014) which receives its funding from DRI Ltd, funded by the UK Medical Research Council, Alzheimer's Society and Alzheimer's Research UK. https://ukdri.ac.uk/ F.K.W. and E.M.C.F. also received funding that contributed to the work in this paper from the MRC via CoEN award MR/S005145/1. https://www.coen.org/ E.M.C.F. received funding from a Wellcome Trust Strategic Award (grant number: 098330/Z/12/Z) awarded to The London Down Syndrome (LonDownS) Consortium and a Wellcome Trust Joint Senior Investigators Award (grant numbers: 098328, 098327). https://wellcome.org/ DM is supported by NIHR GOSH BRC award 17DD08. https://www.nihr.ac.uk/ The funders had no role in study design, data collection and analysis, decision to publish, or preparation of the manuscript.

Competing interests: F.K.W. has undertaken consultancy for Elkington and Fife Patent Lawyers unrelated to the work in the manuscript and is also a PLoS ONE Academic Editor. This does not alter our adherence to PLoS ONE policies on sharing data or materials

through the action of different secretases. The most common processing pathway is 'non-amyloidogenic', which principally occurs at the plasma membrane and consists of sequential cleavage by α- and γ-secretases. The second 'amyloidogenic' pathway leads to the production of amyloid-β, mainly occurs in endosomes and is mediated by sequential cleavage of APP by β- and γ-secretases [8, 9]. Cleavage by β-secretase occurs first, and results in the production of an extracellular fragment that is released from the cell (sAPPβ) and a transmembrane fragment (β-CTF), which is then cleaved by γ-secretase to produce amyloid-β.

Endosomal dysfunction and enlargement is observed in the brains of people who have AD and DS before amyloid-β plaque accumulation and has been suggested to be a key factor in AD development [10–12]. Indeed this has been reported in early gestation of individuals with DS [10, 11], in cells isolated from individuals with DS [13], in iPSCs-derived trisomy-21 neurons and organoids [14–16], and in mouse models of DS [17, 18]. Whether this enlargement is caused by an increased fusion of endosomal bodies or an increase in the volume of single endosomes is disputed [19], likely because of the technical challenges encountered in the precise quantification of the very small endosomal bodies [20–22].

APP triplication is necessary for early endosomal dysfunction in DS models and is mediated by raised β-CTF [17, 21]. Other Hsa21 genes/proteins may also contribute to this dysfunction [17, 23]. For example, synaptojanin-1 (*SYNJ1*), is a phosphatase that mediates the uncoating of clathrin-coated vesicles. SYNJ1 levels are increased in the brains of people who have DS, and its overexpression causes endosomal enlargement [23]. The Hsa21 gene Intersectin-1 (*ITSN1*) encodes a regulator of endocytosis [24] and its levels are increased in DS [25]. Overexpression of the Regulator of Calcineurin 1 (*RCAN1*) affects vesicle recycling and endocytosis via its effect on calcineurin activity [26]. Finally, the Hsa21 microRNA gene *miR-155* negatively regulates the transcription of SNX27, a component of the retromer complex, and SNX27 levels are decreased in DS [27]. Since APP is subject to retrograde transport, impairment of this mechanism could lead to a longer residency of APP inside early endosomes, causing a change in early endosome structure, increased amyloidogenic processing of APP and modifying APP half-life [28].

In addition, research in preclinical systems suggests that genes on Hsa21 including *DYRK1A* and *BACE2* can modulate APP/Aβ biology when in three-copies [17, 29, 30]. Overexpression of DYRK1A in the brain of APP transgenic mice increases the total abundance of APP and Aβ via phosphorylation of APP at Thr668. BACE2 predominantly functions as θ-secretase but may also degrade Aβ or cleave APP at the β-secretase site [31–33]. A recent study in organoids generated from trisomy 21 iPSCs demonstrated that three copies of *BACE2* protect against amyloid-β accumulation in that system [16]. These findings are consistent with gene-association studies implicating these genes in AD-risk in individuals who have DS [34–36].

Here, we investigate whether a novel cellular model of DS that carry three copies of 148 mouse genes that are homologous with Hsa21 genes, including *App*, *Synj1*, *Itsn1*, *Rcan1*, *Mir155*, *Dyrk1A* and *Bace2*, can be used to study APP/amyloid-β and endosomal biology.

Results

Three copies of Hsa21 gene homologues in Dp1Tyb mouse embryonic fibroblasts do not alter endosome numbers

We aimed to determine if an additional copy of Hsa21 homologues was sufficient to increase the number or size of endosomes in mouse embryonic fibroblasts (MEFs) derived from segmental duplication mouse models of DS. Therefore, we established a systematic workflow for quantification of the number and the size distribution of early endosomes, using RAB5

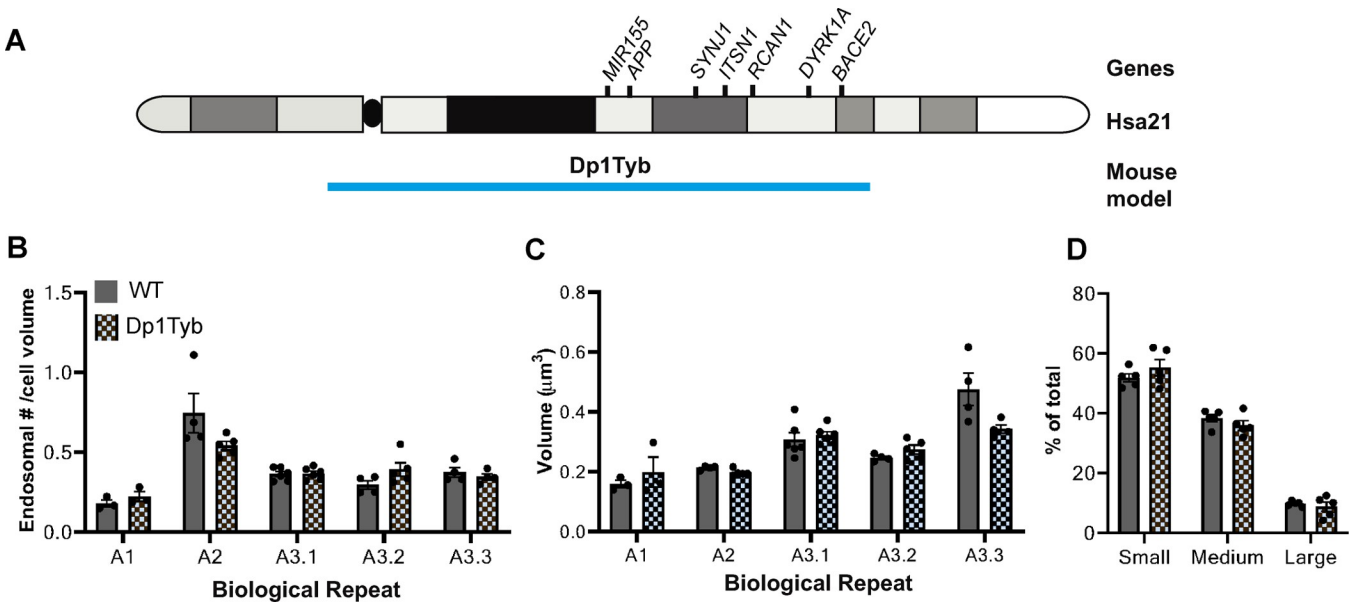

Fig 1. Number of endosomes per cell, endosomal volume distribution and mean volume of the largest endosomes are not different in WT and Dp1Tyb MEFs. A) Schematic of gene content of Dp1Tyb mouse model. **B)** No difference was found in the number of RAB5$^+$ endosomes (normalised to cell volume) in WT and Dp1Tyb MEFs (Nested t-test $p = 0.83$, N = 5 biological repeats, N = 3–5 technical repeats). **C-D)** Endosomes were binned in three size categories: small (0-50th percentile of WT MEFs), medium (50-90th percentile of WT MEFs) and large (90-100th percentile of WT MEFs). The categories were determined using the endosomes in WT MEFs. **C)** No difference in RAB5$^+$ endosome volume distribution was observed in WT and Dp1Tyb MEFs (Mann-Whitney U test). N = 5 biological repeats, N = 3–5 technical repeats. **D)** Volume of the RAB5$^+$ endosomes classified as 'large' is not different in WT and Dp1Tyb MEFs (Nested t-test, $p = 0.21$). N = 5 of biological repeats (independent MEF lines), N = 3–5 technical repeats. *Error bars* = *SEM*.

https://doi.org/10.1371/journal.pone.0262558.g001

staining, confocal imaging and deconvolution (S1 Fig). This workflow was validated by the over-expression of GFP-Rab5CA (Q79L) (RAB5CA), [37]) in wildtype (WT) MEFs (S2 Fig), leading to the expression of constitutively active RAB5, which enlarges endosomal bodies.

We then used this system to study MEFs derived from the Dp(16Lipi-Dbtb21)1TybEmcf [herein referred to as Dp1Tyb] hemizygous mouse model of DS. The Dp1Tyb mouse has a segmental duplication of mouse chromosome 16 (Mmu16) that is homologous with Hsa21 and has an additional copy of 148 mouse Mmu16 genes [38, 39], including *App*, *Synj1*, *Itsn1*, *Rcan1*, *Mir155*, *Dyrk1A* and *Bace2* (Fig 1A).

Using our workflow, we found no difference in the number of RAB5$^+$ endosomes normalised to cell volume in WT and Dp1Tyb MEFs (WT = 2218 ± 58; Dp1Tyb = 2503 ± 119, N = 5 biological repeats) (Fig 1B). Biological variation in the number of RAB5$^+$ endosomes was observed between MEF isolates from individual litters of mice. Therefore, a nested design was used for our onward analysis, enabling us to compare the two genotypes while accounting for the variability between litters.

Three copies of Hsa21 mouse homologues in Dp1Tyb MEFs do not increase endosomal volume

Using our workflow, we determined the volume distribution of RAB5$^+$ endosomes in WT and Dp1Tyb MEFs. The average volume for the total number of endosomes was consistent with our initial pipeline studies in WT MEFs (WT = 0.07 ± 0.001 µm^3, Dp1Tyb = 0.06 ± 0.001 µm^3). WT MEFs isolated from the littermates of the segmental duplication mice were used to determine the 50th and 90th percentile values of endosomal volumes. These data were used to classify endosomes from both genotypes as small (0–50th percentile),

medium (50–90th percentile) and large (> 90th percentile). No difference in size distribution was found between WT and Dp1Tyb MEFs. The average volume of endosomes classified as 'large' was compared and no difference was found between WT and Dp1Tyb MEFs (average volume of large endosomes: WT = 0.29 ± 0.006 μm^3, Dp1Tyb = 0.27 ± 0.003 μm^3 N = 5 biological repeats) (**Fig 1C and 1D**).

Three-copies of *App* do not lead to raised APP protein level or altered half-life in the Dp1Tyb MEF model system

Previous work has suggested that three copies of *APP* and the resulting raised levels of both APP protein and the APP cleavage product β-CTF, are critical to the enlargement of early endosomes in the context of DS [40]. Thus, we investigated whether three copies of *App* were sufficient to raise APP protein level and alter its half-life in the Dp1Tyb MEFs. We crossed the Dp1Tyb mouse model with a heterozygous *App* knockout animal App^{tm1Dbo} ($App^{+/-}$) to generate MEFs and studied three of the resulting genotypes: Dp1Tyb with 3 copies of *App* (Dp1Tyb), Dp1Tyb/$App^{+/-}$ with 2 copies of *App* and WT with 2 copies of *App*.

MEFs with the three genotypes were treated with cycloheximide and collected at 0 h, 15 min, 30 min, 1 h, 2 h and 4 h. APP protein abundance at each time point was measured by western blotting and a non-linear regression test was used to determine APP half-life. We found no difference in APP abundance or APP half-life in Dp1Tyb, Dp1Tyb/$App^{+/-}$ and WT MEFs. This suggests that trisomy of Hsa21-homologous genes on Mmu16, including *App*, is not sufficient to increase APP protein level in this cellular model, and that this dosage-insensitivity is not the result of an increase in the degradation rate of the protein (**Fig 2A–2C**).

Three-copies of Hsa21 mouse homologues in the Dp1Tyb region do not alter amyloid-β production or peptide ratios

Trisomy of genes on Hsa21 other than *App* can modulate the ratio of amyloid-β in vivo [2]. Levels of amyloid-β produced from the endogenous mouse *App* gene were below the limit of detection in MEF culture media. Therefore, to determine if peptide ratios were altered we transfected MEFs with a human βCTF-3xFLAG plasmid to overexpress APP-β-CTF and we quantified the resultant abundance of human amyloid-β. The absolute concentrations of amyloid-β_{40} and amyloid-β_{42} and the ratio of the two peptides were not altered (N = 3) (**Fig 3A–3C**). Amyloid-β_{38} levels were below the limit of detection and were not analysed.

Discussion

Here we compared the biology of early endosomes and APP in MEFs isolated from the Dp1Tyb mouse model. We aimed to determine if this system can be used to investigate the Hsa21 genes responsible for the changes to early endosomes and APP biology that occur in DS. Moreover, the workflow described here may be useful for the systematic quantification of $RAB5^+$ endosome size and number in other cellular models as an alternative to the use of electron microscopy. We found that this DS MEF model did not recapitulate endosomal enlargement, likely because of the dosage insensitivity of *App* in this system. This is consistent with a previous report that showed raised levels of the *App* gene product β-CTF are necessary for DS-associated endosomal enlargement [40].

Since MEFs are embryonic peripheral cells, further changes to biology may be observed in neuronal cells or in the context of aging. However, cellular dysfunction, including in the endo-lysosomal system, occurs in iPSCs, organoids, fibroblasts and lymphoblastoid cells isolated from individuals with DS [13, 15, 23, 41]. Thus differences in human and mouse fibroblast

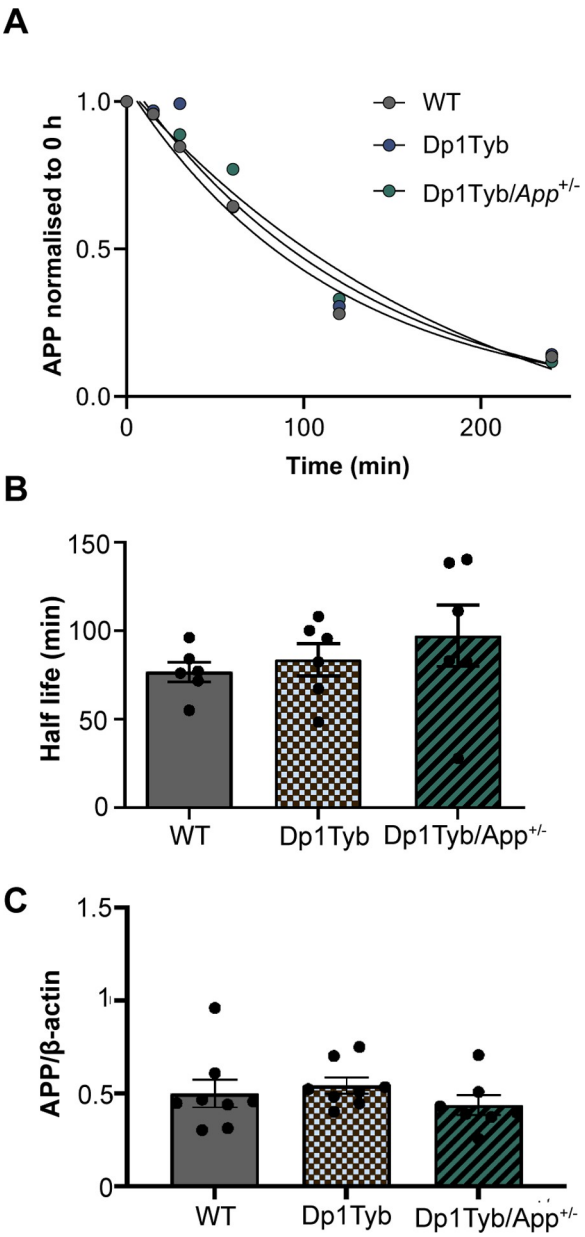

Fig 2. Trisomy of Hsa21-homologous genes including or excluding *App* does not affect APP half-life in MEFs. A) Degradation curve of APP in Dp1Tyb, Dp1Tyb/*App*$^{+/-}$ and WT MEFs. B) Half-life of APP is not significantly different in Dp1Tyb, Dp1Tyb/*App*$^{+/-}$ and WT MEFs (One-way ANOVA, $p = 0.48$, N = 5/6). Average APP half-life in minutes: Dp1Tyb = 84 ± 9; Dp1Tyb/*App*$^{+/-}$ = 97 ± 17; WT = 77 ± 6). C) APP abundance is not significantly different in Dp1Tyb, Dp1Tyb/*App*$^{+/-}$ and WT MEFs (One-way ANOVA, $p = 0.77$, N = 6). Average APP/β-actin: Dp1Tyb = 0.93 ± 0.07; Dp1Tyb/*App*$^{+/-}$ = 0.83 ± 0.1; WT = 0.93 ± 0.15). Each dot corresponds to a biological repeat (i.e. an independent MEF line used). For each biological repeat, three technical repeats (i.e. western blot) were performed. Error bars = SEM. All full uncropped western blots are available at Figshare 10.6084/m9.figshare.17316434.

https://doi.org/10.1371/journal.pone.0262558.g002

biology are likely to underlie our observation that in MEFs isolated from two DS mouse models no alteration in endosomal biology was detected. Endosome enlargement is reported to occur both in the entorhinal cortex and medial septum in the Dp1Yey DS mouse model, which is genetically similar to the Dp1Tyb model [18]. This suggests that differences in the biology between fibroblasts and cells within these brain regions influence this important DS

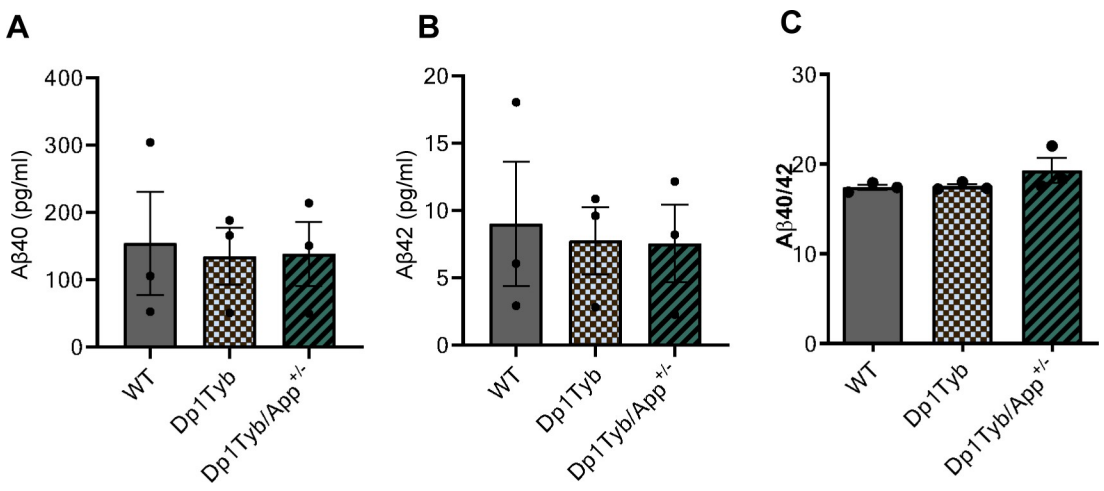

Fig 3. Trisomy of Hsa21-homologous genes, including or excluding *App*, does not affect Aβ40/Aβ42 ratio. In WT, Dp1Tyb and Dp1Tyb/*App*$^{+/-}$ MEFs overexpressing APP-β-CTF led to no difference in **A)** Aβ40 abundance (Dp1Tyb = 134.9 ± 42.5; Dp1Tyb/*App*$^{+/-}$ = 138.2 ± 47.75; WT = 154.1 ± 76.59. One-way ANOVA, $p = 0.97$, N = 3); **B)** Aβ42 abundance (Dp1Tyb = 7.78 ± 2.5; Dp1Tyb/*App*$^{+/-}$ = 7.56 ± 2.88; WT = 9.02 ± 4.61 in pg/ml. One-way ANOVA, $p = 0.95$, N = 3) or **C)** Aβ40/Aβ42 ratio (Dp1Tyb = 17.51 ± 0.24; Dp1Tyb/*App*$^{+/-}$ = 19.29 ± 1.37; WT = 17.38 ± 0.31. One-way ANOVA, $p = 0.26$, N = 3). Each dot corresponds to a biological repeat using an independent MEF lines. Error bars = SEM.

https://doi.org/10.1371/journal.pone.0262558.g003

associated phenotype. This could include differences in the abundance of APP, and β- and γ-secretases between cell types in the mouse. This is consistent with our observation of a lack of detectable CTF-β in MEFs by western blot (10.6084/m9.figshare.17316434).

Future research could quantify APP expression in Dp1Tyb primary neurons to determine whether the lack of *App* dosage sensitivity in MEFs is a result of the embryonic origin of the cells, or because of cell-type specific biology. Previous studies have been inconsistent on the dosage sensitivity of *APP* in different tissues and models, suggesting that APP production is tightly regulated [18, 42–44]. Since three copies of *APP* are sufficient for AD development and APP is the precursor of amyloid-β [1], studying the regulation of APP expression in different tissues and over time could be pivotal to gain further understanding of AD. Our data indicate that in MEFs the endogenous CTF-β level is very low and that 3-copies of *App* are not sufficient to raise the protein above the limit of detection. In the future, Dp1Tyb and WT MEFs could be transfected with CTF-β to determine if an additional dose of other Hsa21 genes modulate the effect of raised CTF-β on endosomal biology, or this could be studied in cell types in which APP/CTF-β are raised in the presence of 3-copies of *App*.

To further investigate APP processing *in vitro* we determined the ratio of amyloid-β_{40} and amyloid-β_{42} peptides and their absolute abundances in MEFs transfected with human β-CTF. The amyloid-β_{40}/amyloid-β_{42} ratio was not altered in Dp1Tyb or Dp1Tyb/*App*$^{+/-}$ MEFs compared to WT controls. This suggests that the additional copy of genes in this region is not sufficient to modulate the processing of APP-CTF to form amyloid-β in fibroblasts. Alić et al. (2020) observed that organoids trisomic for Hsa21 also failed to show an alteration in amyloid-β_{40}/amyloid-β_{42} ratio, but the authors observed an increase in the absolute concentration of amyloid-β_{40} and amyloid-β_{42} produced, together with an increase in total APP which we did not observe in our mouse derived model system. Future research could use brain tissue from Dp1Tyb mice to verify that APP, amyloid-β_{40} and amyloid-β_{42} abundance is increased in the mouse model and the lack of dosage sensitivity is a feature of MEFs. Use of brain tissue at different time points could enable investigation of the progressive changes over life-span,

which cannot be investigated using primary cells. In addition, the Dp1Tyb mouse model contain three copies of a number of mouse homologous chromosome 21 genes, which make them more physiologically relevant than single-gene transgenic models [45].

In conclusion, alternative models to the MEF system investigated here are required to understand how additional copies of genes on Hsa21 change endo-lysosomal and APP biology. These biological processes are proposed to underlie the early development of AD in people who have DS and the identification of alternative model systems will further understanding of this important research area.

Material and methods

Mouse breeding and husbandry

This study was conducted in accordance with ARRIVE2.0 [45]. The mice involved in this study were housed in controlled conditions in accordance with Medical Research Council guidance (*Responsibility in the Use of Animals for Medical Research*, 1993), and experiments were approved by the Local Ethical Review panel (MRC Prion Unit, University College London) and conducted under License from the UK Home Office, according to the revised Animals (Scientific Procedures) Act 1986.

Cage groups and genotypes were pseudo-randomised, with a minimum of two mice and a maximum of five in each cage; groups were weaned with members of the same sex. Mouse houses, bedding and wood chips, and continual access to water were available to all mice, with RM3 and RM1 chow (Special Diet Services, UK) provided to breeding and stock mice, respectively. The water provided was reversed osmosis (RO water). Cages were individually ventilated in a specific pathogen-free facility. Mouse used to generate the breeding stock for this study were euthanised by exposure to a rising concentration of CO_2 gas followed by confirmation of death by dislocation of the neck, according to the revised Animals (Scientific Procedures) Act 1986. The animal facility was maintained at a constant temperature of 19–23˚C with 55 ± 10% humidity in a 12 h light/dark cycle.

Dp(16Lipi-Dbtb21)1TybEmcf [Dp1Tyb] (MGI:5703853) mice were imported from the Francis Crick Institute and colonies were maintained by backcrossing to C56BL/6J. B6.129S7-*App*^{tm1Dbo}/J [*App*$^{+/-}$] (MGI:2136847) mice were imported from the Jackson Laboratory and the colony was maintained by crossing heterozygous knockouts with C57BL/6J animals. To generate progeny for the MEFs used in this project Dp1Tyb mice were crossed with *App*$^{+/-}$ or C57BL/6J mice. Dp1Tyb, *App*$^{+/-}$ colonies were fully inbred for >10 generations on the C57BL/6J genetic background.

Mouse embryonic fibroblasts (MEFs)

Mouse Embryonic Fibroblasts were generated from timed matings; at E14 pregnant females and embryos were culled by a schedule one method. Briefly, the pregnant female mouse in the mating was euthanized, and dissection for the collected embryos was carried out under sterile condition in a laminar flow hood. The uterine horn was dissected and rinsed in 70% ethanol (v/v) and placed into a 100 mm Petri dish. Each embryo was separated from its placenta and embryonic sac. The embryo was decapitated and the head and body were transferred to a 1.5 ml Eppendorf tube containing PBS and delivered for genotyping (heads) and MEF generation (bodies). Red organs were removed from embryo bodies and remaining tissue was minced with 0.25% trypsin-EDTA prior to dissociation by pipetting, cells were isolated by centrifugation and plated on 0.1% gelatin-coated plates in DMEM + GlutaMax, 10% FBS and 1% Penicillin-streptomycin (culture at 37˚C in 5% CO_2).

Genotyping

Genotyping of Dp1Tyb, *App*$^{+/-}$, and Dp1Tyb/*App*$^{+/-}$ mice was outsourced to TransnetYX (Cordova TN, USA) using a proprietary qPCR-based system.

Generation of the βCTF-3xFLAG plasmid, the GFP-Rab5CA plasmid and nucleofection

Briefly, the β-CTF sequence was amplified from a human βCTF-EGFP plasmid (kind gift of Dr Jiang (New York University, USA), then ligated into a pCI-Neo vector. Then the APP signal peptide sequence was ligated into the 5' region and the 3xFLAG into the 3' region. GFP-Rab5CA (Q79L) (RAB5CA), was a kind gift from Sergio Grinstein (University College London, UK) sourced from Addgene (Addgene plasmid # 35140; http://n2t.net/addgene:35140; RRID:Addgene_35140 [37]). These plasmids were transfected into TOP10 competent cells under ampicillin selection and DNA was prepared from cultures with a QIAprep Spin Miniprep Kit (QIAGEN) according to manufacturer's instructions. An Amaxa Nucleofector 2b Device and a Mouse Embryonic Fibroblast Nucleofector Kit 1 (Lonza) were used to transfect MEFs with βCTF-3xFLAG plasmid using program N-024 of the Nucleofector (**S3 Fig**).

Cycloheximide pulse chase

13 h after plating, MEF media was changed and cycloheximide solution (30 μg/ml per well) or ddH_2O (negative control) were added. Cells were collected at 6 timepoints from cycloheximide addition: 0 h, 15 min, 30 min, 1 h, 2 h, 4 h in ice-cold RIPA buffer (150 mM sodium chloride, 50 mM Trizma hydrochloride, 1% NP-40, 0.5% sodium deoxycholate, 0.1% SDS) + 1:100 protease inhibitor (Protease inhibitor cocktail I). The cell suspension was centrifuged for 15 min at 24 000 rcf at 4˚C. APP abundance at each timepoint was normalized to the value at time 0 h. Half-life was calculated using the One Phase Decay (nonlinear regression) function on GraphPad Prism. The values obtained for each technical repeat (i.e. gel) were averaged together to obtain one half-life value per genotype per experimental repeat, such that independent biological replicates were used as the experimental unit. These values were then compared with a one-way ANOVA test on GraphPad Prism.

Aβ peptides measure

The Mesoscale amyloid-β 6E10 Triplex Assay (Meso Scale Discovery, MSD) was used to determine the concentration of amyloid-β isoforms (amyloid-β_{38}, amyloid-β_{40}, amyloid-β_{42}) in media collected from MEFs and diluted 1:2 in Dilutor 35. A MESO SECTOR S 600 plate reader (MSD) was used to read the plate.

Western blotting

Pierce 660nm Protein Assay Reagent was used to measure protein concentrations using a standard of Bovine Serum Albumin (BSA) in PBS (3000–0 μg/ml). Samples were denatured in NuPAGE LDS 4X and 2-mercaptoethanol by boiling at 95˚C for 5 min. Bolt 4–12% Bis-Tris Plus Gels and Bolt MES SDS Running Buffer 20X were used for protein separation before transfer to 0.2 μm nitrocellulose membranes (Transblot Turbo Transfer Pack, Bio-Rad) using a Transblot Turbo (Bio-Rad). Proteins were blocked in 5% skimmed milk in PBS prior to incubation with primary antibody (anti-APP A8717 1:5000 Sigma Aldrich) at 4˚C overnight prior to incubation with anti-rabbit HRP. Membranes were developed using Super Signal West Pico

Chemiluminescent Substrate. ImageJ was used to quantify the signal from bands and the linearity of APP signal was confirmed by western blot of endogenous APP (doubling-dilutions).

Immunocytochemistry

Cells were washed in PBS then fixed in 4% PFA for 20 min prior to permeabilization with 0.05% saponin/PBS for 10 min. Cells were blocked with 5% BSA/PBS for 1 h before overnight incubation with primary antibodies in 1% BSA/PBS (RAB5 21435 1:200 Cell Signalling and anti-Integrin-β1 MAB1997 1:1000, Millipore) at 4˚C prior to washing and incubation with secondary antibodies (anti-rabbit AlexaFluor-546 [A11-35] and anti-mouse AlexaFluor-633 [A21052] Thermofisher) in 1% BSA/PBS. Cells were mounted on SuperFrost adhesion slides (VWR International) with ProlongGold + DAPI.

Imaging

Images were taken on Confocal microscope Zeiss Examiner LSM880. Each image was taken with a 63x1.4 Oil Plan Apochromat objective in two channels. Z-stacks at 150 nm interval between slices were taken to include the whole cell. Pixel size was equal to x, y = 0.05 μm, z = 0.15 μm. The pinhole size was equal to 1 Airy Unit of the 546 channel. Deconvolution for RAB5 signal was performed with Huygens software signal/noise ratio = 15. ImageJ software was used to clear the space surrounding the cells and to measure their volume. Briefly, the surface of the cell was smoothed and thresholded in 3D; everything outside the cell was cleared, using a custom macro (S4 Fig). Imaris software was used to build a 3D reconstruction of the staining after deconvolution. Objects were identified using the surfaces function, with smoothing disabled and thresholding with background subtraction using default settings. This allowed us to make an accurate measurement of a large number of endosomes in three dimensions. Volume data were generated by the software and imported in excel. Endosomal volume (μm^3) was used to calculate endosomal size. The size parameters of endosomes between the 50th and 90th percentiles were determined in WT MEFs transfected with PBS, and this information was used to classified endosomes in small (0-50th percentile), medium (50-90th percentile) and large (90-100th percentile) bins. A nested ANOVA was used to compare the size of large endosomes in MEFs transfected with PBS vs RAB5. Raw lsm/czi files available at https://www.ebi.ac.uk/biostudiesTMP_1647346060608.

Experimental design and statistical analysis

Sample size was determined by a power calculation using pilot data. Sample order in all experiments (including during culture, western blotting and MSD assay) was randomized but balanced by genotype. All experiments and data analysis undertaken blind to genotype. All statistical tests were performed with IBM SPSS Statistics Version 2.5 and GraphPad Prism Version 8.4.2. All data is reported as mean ± SEM. All data was checked for normality of distribution and homogeneity of samples; sample distribution was tested with a Levene's test, and data normality was tested with a Kolmogorov-Smirnov test. If the assumptions of normality and homogeneity of variance were verified, parametric tests were used to analyse data; otherwise non-parametric tests were used. For each experiment, the effect of genotype and sex was assessed using a multivariate ANOVA test. If the effect of one or more of the variables was significant, the variable was tested separately using ANOVA test, t-test or their non-parametric equivalents.

Supporting information

S1 Fig. Process of quantification of RAB5$^+$ endosomal staining. A) WT MEF stained for Integrinβ (cell membrane, green) and RAB5 (endosomes, red). **B, D)** Endosomal staining after

deconvolution and background clearance **C, E)** 3D reconstruction of endosomal staining. Deconvolution and 3D reconstruction to accurately quantify the volume of endosomes. Z-stacks of each cell were taken with 150 nm interval between slices and fixed voxel volume (x = 50 nm, y = 50 nm, z = 150 nm) on confocal microscope LSM880. Each stack was deconvolved using Huygens software to improve image signal to noise and resolution. ImageJ software was used to remove the background with a macro written by Dr Dale Moulding. Imaris software was used to reconstruct the deconvolved staining in 3D. The area of Integrinβ was used to create a mask to define cellular volume.
(TIF)

S2 Fig. Distribution and quantification of endosomes in MEFs transfected with PBS and RAB5CA. A) The normal distribution of endosomal size in WT MEFs transfected with PBS was determined to define the parameters for classification of "large" endosomes (small: endosomes in the 0–50th percentile, medium: endosomes in the 50–90th percentile, large: endosomes in the >90thpercentile). **B)** A nested t-test showed that 'large' endosomes in cells transfected with RAB5CA had a significantly higher volume than the endosomes in cells transfected with PBS ($p = 0.007$, N = 3 of biological repeats). *The dots indicate the average volume of the 'large' endosomes in one cell imaged (technical repeat). Error bars = SEM*. **C, D)** Representative images of WT MEFs transfected with PBS (**C**) or RAB5CA (**D**), endosomes labelled with RAB5 antibody (red), the RAB5CA plasmid is GFP-tagged (green); enlarged endosome indicated with (white arrow).
(TIF)

S3 Fig. Detail of the pCI-neo βCTF-3xFLAG plasmid map. The APP signalling sequence was inserted in a pCI-neo plasmid followed by the β-CTF fragment of APP and by a 3xFLAG sequence. The primers used for sequencing the insert (*sequencing forward and reverse*) are also shown.
(TIF)

S4 Fig. Custom ImageJ Macro. Macro designed by Dr Dale Moulding to smooth the cell surface and clear its outside in 3D, enabling accurate quantification of the volume of the cell and of the number and volume of endosomes.
(PDF)

Acknowledgments

The LonDownS Consortium is led by Andre Strydom (andre.strydom@kcl.ac.uk)[1,2], and comprises of Elizabeth M.C. Fisher[3], Frances K. Wiseman[4], Dean Nizetic[5,6], John Hardy[4,7], Victor L. J. Tybulewicz[8,9] and Annette Karmiloff-Smith[10]. [1]Department of Forensic and Neurodevelopmental Sciences, Institute of Psychiatry, Psychology and Neuroscience, King's College London, London, UK. [2]Division of Psychiatry, University College London, London, UK. [3]Department of Neuromuscular Diseases, Queen Square Institute of Neurology, University College London, Queen Square, London, UK. [4]The UK Dementia Research Institute, University College London, Queen Square, London, UK. [5]Blizard Institute, Barts and the London School of Medicine, Queen Mary University of London, London, UK. [6]Lee Kong Chian School of Medicine, Nanyang Technological University, Singapore, Singapore. [7]Reta Lila Weston Institute, Institute of Neurology, University College London, London, London, UK. [8]The Francis Crick Institute, London, UK. [9]Department of Immunology and Inflammation, Imperial College, London, UK. [10]Birkbeck University, London, UK.

We thank Amanda Heslegrave (UCL-DRI) for assistance with this project.

F.K.W. has undertaken consultancy for Elkington and Fife Patent Lawyers unrelated to the work in the manuscript and is also a PLoS ONE Academic Editor. This does not alter our adherence to PLoS ONE policies on sharing data or materials.

Author Contributions

Conceptualization: Frances K. Wiseman.

Data curation: Paige Mumford, Frances K. Wiseman.

Formal analysis: Claudia Cannavo.

Funding acquisition: Elizabeth M. C. Fisher, Frances K. Wiseman.

Investigation: Claudia Cannavo, Karen Cleverley, Cheryl Maduro, Paige Mumford.

Methodology: Dale Moulding.

Project administration: Elizabeth M. C. Fisher, Frances K. Wiseman.

Resources: Dale Moulding, Elizabeth M. C. Fisher.

Software: Dale Moulding.

Supervision: Dale Moulding, Elizabeth M. C. Fisher, Frances K. Wiseman.

Writing – original draft: Claudia Cannavo, Frances K. Wiseman.

Writing – review & editing: Paige Mumford, Dale Moulding, Elizabeth M. C. Fisher, Frances K. Wiseman.

References

1. Wiseman FK, Al-Janabi T, Hardy J, Karmiloff-Smith A, Nizetic D, Tybulewicz VLJ, et al. A genetic cause of Alzheimer disease: Mechanistic insights from Down syndrome. Nature Reviews Neuroscience. 2015. pp. 564–574. https://doi.org/10.1038/nrn3983 PMID: 26243569
2. Wiseman FK, Pulford LJ, Barkus C, Liao F, Portelius E, Webb R, et al. Trisomy of human chromosome 21 enhances amyloid-β deposition independently of an extra copy of APP. Brain. 2018; 141: 2457–2474. https://doi.org/10.1093/brain/awy159 PMID: 29945247
3. Thinakaran G, Koo EH. Amyloid Precursor Protein Trafficking, Processing, and Function. J Biol Chem. 2008; 283: 29615–29619. https://doi.org/10.1074/jbc.R800019200 PMID: 18650430
4. Jiang S, Li Y, Zhang X, Bu G, Xu H, Zhang YW. Trafficking regulation of proteins in Alzheimer's disease. Molecular Neurodegeneration. BioMed Central; 2014. p. 6. https://doi.org/10.1186/1750-1326-9-6 PMID: 24410826
5. Haass C, Kaether C, Thinakaran G, Sisodia S. Trafficking and proteolytic processing of APP. Cold Spring Harb Perspect Med. 2012; 2. https://doi.org/10.1101/cshperspect.a006270 PMID: 22553493
6. Plácido AI, Pereira CMF, Duarte AI, Candeias E, Correia SC, Santos RX, et al. The role of endoplasmic reticulum in amyloid precursor protein processing and trafficking: Implications for Alzheimer's disease. Biochim Biophys Acta—Mol Basis Dis. 2014; 1842: 1444–1453. https://doi.org/10.1016/j.bbadis.2014.05.003 PMID: 24832819
7. Perez RG, Soriano S, Hayes JD, Ostaszewski B, Xia W, Selkoe DJ, et al. Mutagenesis identifies new signals for β-amyloid precursor protein endocytosis, turnover, and the generation of secreted fragments, including Aβ42. J Biol Chem. 1999; 274: 18851–18856. https://doi.org/10.1074/jbc.274.27.18851 PMID: 10383380
8. Kaether C, Schmitt S, Willem M, Haass C. Amyloid precursor protein and Notch intracellular domains are generated after transport of their precursors to the cell surface. Traffic. 2006; 7: 408–415. https://doi.org/10.1111/j.1600-0854.2006.00396.x PMID: 16536739
9. Das U, Wang L, Ganguly A, Saikia JM, Wagner SL, Koo EH, et al. Visualizing APP and BACE-1 approximation in neurons yields insight into the amyloidogenic pathway. Nat Neurosci. 2015; 19: 55–64. https://doi.org/10.1038/nn.4188 PMID: 26642089

10. Cataldo AM, Barnett JL, Pieroni C, Nixon RA. Increased neuronal endocytosis and protease delivery to early endosomes in sporadic Alzheimer's disease: Neuropathologic evidence for a mechanism of increased β-amyloidogenesis. J Neurosci. 1997; 17: 6142–6151. https://doi.org/10.1523/JNEUROSCI.17-16-06142.1997 PMID: 9236226

11. Cataldo AM, Peterhoff CM, Troncoso JC, Gomez-Isla T, Hyman BT, Nixon RA. Endocytic pathway abnormalities precede amyloid β deposition in sporadic alzheimer's disease and down syndrome: Differential effects of APOE genotype and presenilin mutations. Am J Pathol. 2000; 157: 277–286. https://doi.org/10.1016/s0002-9440(10)64538-5 PMID: 10880397

12. Small SA, Petsko GA. Endosomal recycling reconciles the Alzheimer's disease paradox. Sci Transl Med. 2020; 12. https://doi.org/10.1126/scitranslmed.abb1717 PMID: 33268506

13. Cataldo AM, Mathews PM, Boiteau AB, Hassinger LC, Peterhoff CM, Jiang Y, et al. Down syndrome fibroblast model of Alzheimer-related endosome pathology: Accelerated endocytosis promotes late endocytic defects. Am J Pathol. 2008; 173: 370–384. https://doi.org/10.2353/ajpath.2008.071053 PMID: 18535180

14. Israel MA, Yuan SH, Bardy C, Reyna SM, Mu Y, Herrera C, et al. Probing sporadic and familial Alzheimer's disease using induced pluripotent stem cells. Nature. 2012; 482: 216–220. https://doi.org/10.1038/nature10821 PMID: 22278060

15. Raja WK, Mungenast AE, Lin YT, Ko T, Abdurrob F, Seo J, et al. Self-organizing 3D human neural tissue derived from induced pluripotent stem cells recapitulate Alzheimer's disease phenotypes. PLoS One. 2016; 11. https://doi.org/10.1371/journal.pone.0161969 PMID: 27622770

16. Alić I, Goh PA, Murray A, Portelius E, Gkanatsiou E, Gough G, et al. Patient-specific Alzheimer-like pathology in trisomy 21 cerebral organoids reveals BACE2 as a gene dose-sensitive AD suppressor in human brain. Mol Psychiatry. 2020. https://doi.org/10.1038/s41380-020-0806-5 PMID: 32647257

17. Cataldo AM, Petanceska S, Peterhoff CM, Terio NB, Epstein CJ, Villar A, et al. App gene dosage modulates endosomal abnormalities of Alzheimer's disease in a segmental trisomy 16 mouse model of Down syndrome. J Neurosci. 2003; 23: 6788–6792. https://doi.org/10.1523/JNEUROSCI.23-17-06788.2003 PMID: 12890772

18. Sawa M, Overk C, Becker A, Derse D, Albay R, Weldy K, et al. Impact of increased APP gene dose in Down syndrome and the Dp16 mouse model. Alzheimers Dement. 2021 [cited 12 Mar 2022]. https://doi.org/10.1002/alz.12463 PMID: 34757693

19. Botté A, Lainé J, Xicota L, Heiligenstein X, Fontaine G, Kasri A, et al. Ultrastructural and dynamic studies of the endosomal compartment in down syndrome. Acta Neuropathol Commun. 2020; 8. https://doi.org/10.1186/s40478-020-00956-z PMID: 32580751

20. Klumperman J, Raposo G. The complex ultrastructure of the endolysosomal system. Cold Spring Harb Perspect Biol. 2014; 6. https://doi.org/10.1101/cshperspect.a016857 PMID: 24851870

21. Jiang Y, Rigoglioso A, Peterhoff CM, Pawlik M, Sato Y, Bleiwas C, et al. Partial BACE1 reduction in a Down syndrome mouse model blocks Alzheimer-related endosomal anomalies and cholinergic neurodegeneration: Role of APP-CTF. Neurobiol Aging. 2016; 39: 90–98. https://doi.org/10.1016/j.neurobiolaging.2015.11.013 PMID: 26923405

22. Xu W, Weissmiller AM, White JA, Fang F, Wang X, Wu Y, et al. Amyloid precursor protein-mediated endocytic pathway disruption induces axonal dysfunction and neurodegeneration. J Clin Invest. 2016; 126: 1815–1833. https://doi.org/10.1172/JCI82409 PMID: 27064279

23. Cossec JC, Lavaur J, Berman DE, Rivals I, Hoischen A, Stora S, et al. Trisomy for synaptojanin1 in down syndrome is functionally linked to the enlargement of early endosomes. Hum Mol Genet. 2012; 21: 3156–3172. https://doi.org/10.1093/hmg/dds142 PMID: 22511594

24. Yu Y, Chu PY, Bowser DN, Keating DJ, Dubach D, Harper I, et al. Mice deficient for the chromosome 21 ortholog Itsn1 exhibit vesicle-trafficking abnormalities. Hum Mol Genet. 2008; 17: 3281–3290. https://doi.org/10.1093/hmg/ddn224 PMID: 18676989

25. Hunter MP, Nelson M, Kurzer M, Wang X, Kryscio RJ, Head E, et al. Intersectin 1 contributes to phenotypes in vivo: Implications for Down's syndrome. Neuroreport. 2011; 22: 767–772. https://doi.org/10.1097/WNR.0b013e32834ae348 PMID: 21876463

26. Zanin MP, MacKenzie KD, Peiris H, Pritchard MA, Keating DJ. RCAN1 regulates vesicle recycling and quantal release kinetics via effects on calcineurin activity. J Neurochem. 2013; 124: 290–299. https://doi.org/10.1111/jnc.12086 PMID: 23134420

27. Wang X, Zhao Y, Zhang X, Badie H, Zhou Y, Mu Y, et al. Loss of sorting nexin 27 contributes to excitatory synaptic dysfunction by modulating glutamate receptor recycling in Down's syndrome. Nat Med. 2013; 19: 473–480. https://doi.org/10.1038/nm.3117 PMID: 23524343

28. Small SA, Kent K, Pierce A, Leung C, Kang MS, Okada H, et al. Model-guided microarray implicates the retromer complex in Alzheimer's disease. Ann Neurol. 2005; 58: 909–919. https://doi.org/10.1002/ana.20667 PMID: 16315276

29. Ryoo SR, Cho HJ, Lee HW, Jeong HK, Radnaabazar C, Kim YS, et al. Dual-specificity tyrosine(Y)-phosphorylation regulated kinase 1A-mediated phosphorylation of amyloid precursor protein: evidence for a functional link between Down syndrome and Alzheimer's disease. J Neurochem. 2008; 104: 1333–1344. https://doi.org/10.1111/j.1471-4159.2007.05075.x PMID: 18005339

30. Garcia-Cerro S, Rueda N, Vidal V, Lantigua S, Martinez-Cue C. Normalizing the gene dosage of Dyrk1A in a mouse model of Down syndrome rescues several Alzheimer's disease phenotypes. Neurobiol Dis. 2017; 106: 76–88. https://doi.org/10.1016/j.nbd.2017.06.010 PMID: 28647555

31. Voytyuk I, Mueller SA, Herber J, Snellinx A, Moechars D, van Loo G, et al. BACE2 distribution in major brain cell types and identification of novel substrates. Life Sci Alliance. 2018; 1. https://doi.org/10.26508/lsa.201800026 PMID: 30456346

32. Hussain I, Powell DJ, Howlett DR, Chapman GA, Gilmour L, Murdock PR, et al. Asp1 (BACE2) cleaves the amyloid precursor protein at the β-secretase site. Mol Cell Neurosci. 2000; 16: 609–619. https://doi.org/10.1006/mcne.2000.0884 PMID: 11083922

33. Abdul-Hay SO, Sahara T, McBride M, Kang D, Leissring MA. Identification of BACE2 as an avid -amyloid-degrading protease. Mol Neurodegener. 2012; 7. https://doi.org/10.1186/1750-1326-7-46 PMID: 22986058

34. Mok KY, Jones EL, Hanney M, Harold D, Sims R, Williams J, et al. Polymorphisms in BACE2 may affect the age of onset Alzheimer's dementia in Down syndrome. Neurobiol Aging. 2014; 35: 1513.e1-1513.e5. https://doi.org/10.1016/j.neurobiolaging.2013.12.022 PMID: 24462566

35. Kimura R, Kamino K, Yamamoto M, Nuripa A, Kida T, Kazui H, et al. The DYRK1A gene, encoded in chromosome 21 Down syndrome critical region, bridges between β-amyloid production and tau phosphorylation in Alzheimer disease. Hum Mol Genet. 2007; 16: 15–23. https://doi.org/10.1093/hmg/ddl437 PMID: 17135279

36. Lee JH, Lee AJ, Dang LH, Pang D, Kisselev S, Krinsky-McHale SJ, et al. Candidate gene analysis for Alzheimer's disease in adults with Down syndrome. Neurobiol Aging. 2017; 56: 150–158. https://doi.org/10.1016/j.neurobiolaging.2017.04.018 PMID: 28554490

37. Bohdanowicz M, Balkin DM, De Camilli P, Grinstein S. Recruitment of OCRL and Inpp5B to phagosomes by Rab5 and APPL1 depletes phosphoinositides and attenuates Akt signaling. Mol Biol Cell. 2012; 23: 176–187. https://doi.org/10.1091/mbc.E11-06-0489 PMID: 22072788

38. Lana-Elola E, Watson-Scales S, Slender A, Gibbins D, Martineau A, Douglas C, et al. Genetic dissection of Down syndrome- associated congenital heart defects using a new mouse mapping panel. Elife. 2016. https://doi.org/10.7554/eLife.11614 PMID: 26765563

39. Herault Y, Delabar JM, Fisher EMC, Tybulewicz VLJ, Yu E, Brault V. Rodent models in Down syndrome research: impact and future opportunities. Dis Model Mech. 2017; 10: 1165–1186. https://doi.org/10.1242/dmm.029728 PMID: 28993310

40. Jiang Y, Mullaney KA, Peterhoff CM, Che S, Schmidt SD, Boyer-Boiteau A, et al. Alzheimer's-related endosome dysfunction in Down syndrome is Aβ-independent but requires APP and is reversed by BACE-1 inhibition. Proc Natl Acad Sci U S A. 2010; 107: 1630–1635. https://doi.org/10.1073/pnas.0908953107 PMID: 20080541

41. Cossec J-C, Simon A, Marquer C, Moldrich RX, Leterrier C, Rossier J, et al. Clathrin-dependent APP endocytosis and Aβ secretion are highly sensitive to the level of plasma membrane cholesterol. Biochim Biophys Acta—Mol Cell Biol Lipids. 2010; 1801: 846–852. https://doi.org/10.1016/j.bbalip.2010.05.010 PMID: 20580937

42. Engidawork E, Lubec G. Protein expression in Down syndrome brain. Amino Acids. Springer; 2001. pp. 331–361. https://doi.org/10.1007/s007260170001 PMID: 11858695

43. Cheon MS, Dierssen M, Kim SH, Lubec G. Protein expression of BACE1, BACE2 and APP in Down syndrome brains. Amino Acids. 2008; 35: 339–343. https://doi.org/10.1007/s00726-007-0618-9 PMID: 18163181

44. Lyle R, Gehrig C, Neergaard-Henrichsen C, Deutsch S, Antonarakis SE. Gene expression from the aneuploid chromosome in a trisomy mouse model of Down syndrome. Genome Res. 2004; 14: 1268–1274. https://doi.org/10.1101/gr.2090904 PMID: 15231743

45. Choong XY, Tosh JL, Pulford LJ, Fisher EMC. Dissecting Alzheimer disease in down syndrome using mouse models. Frontiers in Behavioral Neuroscience. Frontiers; 2015. p. 268. https://doi.org/10.3389/fnbeh.2015.00268 PMID: 26528151